Fracture Mechanics of Concrete Structures, de Borst et al (eds) © 2001 Swets & Zeitlinger, Lisse, ISBN 90 2651 825 0

Experimental investigation of fracture processes in concrete cylinders subjected to torsion

G.Lilliu & J.G.M.van Mier
Microlab, Faculty of Civil Engineering and Geo-Sciences, Delft University of Technology, Delft, The Netherlands

ABSTRACT: In order to validate the 3D version of the 'Delft' lattice model a number of torsion tests was conducted on concrete cylinders. The cylinders were both notched and un-notched. A biaxial loading machine with rotational and vertical loading axes was used. Tests were conducted under different axial restraint. It was observed that a perturbation of the stress state induced by the torque may significantly affect the crack pattern. Under axial compressive stress, after a spiralling crack, an axial crack developed in un-notched specimens. In notched cylinders, the failure surface is conical if an axial load is present, while it appears flat and localized within the notch height in case no axial load is applied. In order to have a better insight in the fracture process, an impregnation technique is used for detecting the cracks at different stages of loading.

1 INTRODUCTION

At the beginning of the 1990's a 2D lattice model was developed in Delft (Schlangen and van Mier 1992a). In the past ten years this model has been used for simulating experiments on concrete specimens subjected to plane stress. Despite the realistic crack patterns, the response of the model in terms of load-displacement diagrams has always been too brittle when compared with experimental results. Two possible causes were considered. The first was that fracture processes are 3D phenomena. The second was that, in order to limit the computational times, relatively coarse meshes were adopted and the smallest aggregate fractions ($d_a \leq 2$ mm) were neglected. The presence of randomly distributed inclusions in the material produces curvatures of the crack surface in all directions. When small particles are included in the grain structure, the crack pattern becomes more complex, considerable branching and bridging is observed and the resulting post-peak response is more ductile (Schlangen 1993). As a result, the dissipated energy increases. For these reasons a 3D version of the model was developed (Lilliu and van Mier 2000) and implemented in a finite element package for parallel computers (Lingen 2000). In order to validate the 3D lattice model, torsion tests on concrete cylinders are selected. These tests were chosen because of the possibility to obtain crack surfaces that are curved in multiple directions, but the test is interesting in its own right because results affected by combined tensile and shear stresses can be obtained.

Several attempts have been made in the past to design a set-up for conducting torsion experiments on cylinders, e.g. (Xu and Reinhardt 1989; Yacoub-Tokatly, Barr, and Norris 1989; Bažant, Prat, and Tabbara 1990). The main reason for the torsion tests conducted in the early 1990's was to define a macroscopic mode III fracture energy for concrete. In general beam theory is applied to the compact torsion cylinders and also to the compact beam specimens that are often used for the determination of mode II fracture parameters, see for example (Bažant and Pfeiffer 1986). The range of application of beam theory has by far been exceeded in these compact specimens, and the best approach seems to regard the specimen as a three-dimensional structure with its own specific boundary conditions. Two sources of stress-concentrations are present: the heterogeneous material structure, and the boundary conditions of the experiment. The combined effect is a critical stress concentration where failure will initiate. In meso-mechanics models like the lattice model, both sources of stress concentrations are present. So far it has been possible to analyze failure of concrete specimens under a variety of external loading conditions such as the four-point-shear beam (Schlangen and van Mier 1992b), anchor pull-out (Vervuurt, van Mier, and Schlangen 1994), and the Brazilian splitting test (Lilliu and van Mier 1999). Next to the aforementioned brittleness problem in the calculated load-deformation diagrams, the lattice model cannot be applied to compressive failure modes. The torsion tests are useful in this respect as well, since a variety of tensile/compressive failure modes can be obtained, see for example (Bažant, Prat, and Tabbara 1990).

In the paper torque-rotation diagrams and failure patterns from tests on un-notched and notched cylin-

ders under a variety of axial constraint are presented. These results form the basis for validation of the 3D-lattice model, which recently has become available.

2 EXPERIMENTAL DETAILS

Tests were conducted on concrete cylinders with diameter D=34 mm and height H=68 mm. Both un-notched and notched cylinders were used. The notch, at half height of the cylinder, had a depth d_0=8 mm.

The specimens were cored from concrete blocks, casted in plywood moulds. Two mixtures with maximum aggregate size d_a=2 mm and d_a=8 mm, respectively, were used. Here we will discuss the results from the 2 mm mixture only. The cement:sand ratio (by weight) was 1:1.7 and the water/cement ratio 0.4. Portland CEM I 32.5R cement was used. During pouring of the mixture and for other 30 seconds after complete filling, the moulds were vibrated on a small vibrating table. Next, they were covered with plastic sheets. After two days, the concrete blocks were demoulded and placed under water. The cylinders, cored from the concrete blocks after 28 days, were kept in a climate box, at 20^{0}C and 90% RH, till the moment of testing.

The tests were conducted with a servo-hydraulic INSTRON 8874. This machine has rotational and vertical loading axes, which can be coupled or decoupled. The maximum loads which can be reached are 100 Nm and 10 kN, respectively. The feed-back signal during the tests is the rotation, measured with a rotational potentiometer connected to a wire attached to the upper loading platen, as shown in Figure 1.

Different tests with different axial restraint were conducted. The cases considered were: zero axial force, zero axial displacement and constant axial

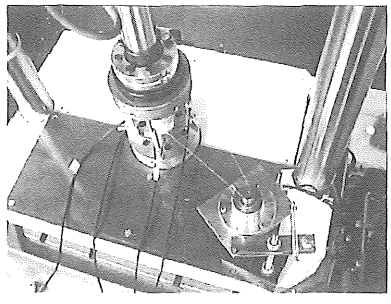

Figure 1. Set-up for measurements of the rotational angle.

compressive force. An hour before testing the specimen was glued to the loading platens. After hardening of the glue, the axial load was applied first, whereafter the rotational load was applied at the constant speed of 0.002 deg/sec. During the tests the stroke (axial displacement measured by the LVDT in the hydraulic actuator), the axial load, the rotation and the torque were recorded.

3 EXPERIMENTAL RESULTS

Two series of tests were conducted and, for each loading condition, three tests. The average of the peak torque and of the axial load, with the corresponding standard deviations, are reported in Table 1 and Table 2, for un-notched and notched cylinders, respectively. There, the tests are named after the applied loading condition: d2f, d2d and d2c refer to tests on cylinders without notch under zero axial force, zero axial displacement and constant axial compression, respectively. In the same way, d2nf, d2nd and d2nc refer to tests on notched cylinders. In Figure 2 and Figure 3 the experimental results are reported, together with some of the obtained crack patterns. The torque versus rotation curves recorded in the first and second series of experiments are represented with a dashed and a continuous line, respectively. Different gradations of grey colour have been used for each test of the series. For the experiments conducted under fixed displacement, the axial load versus rotation curves are represented on top of the torsion versus rotation curves. The crack patterns shown in these figures were photographed from opposite orientations around the specimen, at the stage indicated with a large dot near the end of the torque-rotation diagram represented with the black continuous line.

Table 1. Results of tests on un-notched cylinders.

	peak torque Nm	peak load kN	series	
d2f	69.4 (2.2)	0	1	F_{ax}=0
	66.8*	0	2	
d2d	66.6*	-3.8*	1	δ_{ax}=0
	70.0 (3.3)	-3.5 (0.9)	2	
d2c	95.0 (1.7)	-3.5	1	F_{ax}=comp
	93.6 (3.3)	-3.6	2	

Table 2. Results of tests on notched cylinders.

	peak torque Nm	peak load kN	series	
d2nf	25.1 (1.6)	0	1	F_{ax}=0
	24.4 (0.8)	0	2	
d2nd	48.0 (1.9)	-4.1 (0.6)	1	δ_{ax}=0
	51.7 (1.6)	-4.7 (0.2)	2	
d2nc	42.7*	-1.1	1	F_{ax}=comp
	49.0 (1.0)	-1.1	2	

*Average computed on two tests.

3.1 Un-notched cylinders

Independently from the axial restraint, the crack which can be detected first with the naked eye is that labeled with 1. This crack spirals around the specimen. Since it could be detected only after it covered almost the whole length of the cylinder, it is not sure if it started from one end or within the body of the cylinder. As a matter of fact, according to the solution of the linear elastic problem, the twisting moment is

constant and the crack initiation should be just a consequence of stress concentrations due to the internal structure of the material. However, the specimen is clamped to the loading platens and cannot contract freely. As a consequence, radial tensile stresses might arise at the ends of the specimen, causing crack initiation. Other cracks, labeled with 2 in Figure 2, depart from the spiralling crack as "wings". The spiralling crack can be either continuous or consists of more overlapping branches. In some cases, more than one of such cracks could be detected.

When no axial load is applied, the spiralling crack travels towards the end of the specimen and turns, forming a loop (Fig. 2a). In case of axial restraint, vertical cracks develop, producing even spalling of concrete, as shown in Figure 2c. The cases of zero axial displacement (Fig. 2b) and constant axial compressive load are similar. This is due to the fact that, when the specimen cannot elongate freely, a compressive force arises. Thus, the vertical cracks seem a consequence of the axial compressive stresses, although these are of very limited magnitude (4 MPa).

The torque-rotation diagrams have a peak and a softening branch. The tests stop when the specimen fails or when the external rotation has reached the maximum value, namely 10 deg. When there is no axial load the softening branch is extremely smooth and presents a tail. The shape of the diagrams is somehow more complex when there is an axial restraint. In case of zero axial displacement, the shape of the torque-rotation diagram is somehow related to the shape of the axial load-rotation diagram. The softening branch in the torque-rotation diagram starts when the compressive force has reached the maximum value. After it has reached a minimum, it may either start to increase or form a sort of plateau and, afterwards, descend again. Contrary to the case of zero axial load, some scatter in the diagram shapes can be observed. Namely, the diagram can drop after the peak load or present a rounded peak zone.

In case of compressive load, the diagram drops after the peak and the post-peak region is characterized by changes of slope. After a minimum torque is reached, which might be almost zero, the torque increases again with the rotation. Like in the tests conducted under zero axial displacement, the experimental results present some scatter, specially in the region after the minimum torque has been reached. The presence of a constant compressive load seems to be a very effective confinement and, thus, strengthens the material. In fact, the peak torque is about 30% higher than in the case of zero axial displacement, where the compression varies during the test.

3.2 Notched cylinders

If no axial restraint is applied, the notch causes the localization of the fracture within its height. During the test, it was possible to observe inclined, parallel cracks on the surface of the cylinder's core. Coalescence of such cracks produced the final failure, as shown in Figure 3a. The deep notch creates sufficient confinement for the development of a "shear-like" crack consisting of multiple inclined tensile cracks.

When an axial restraint is applied, cracks are similar to the spiralling cracks observed in the un-notched cylinders and seem to start right at the notch, where they show a wider opening. However, cracks do not localize within the height of the notch, but develop along half of the specimen length. Only in the second series, two of the tests conducted under zero axial displacement showed cracks at both specimen halves. In all the cases considered, a final conical failure surface as reported earlier (Bažant, Prat, and Tabbara 1990) was observed. The cone appeared flatter in the tests conducted under constant compressive force (see Fig. 3c) than in tests under zero axial displacement (see Fig. 3b).

Similar to the tests on un-notched cylinders, in the notched cylinder tests under zero axial displacement a compressive axial force develops. This force increases till a maximum, which corresponds either to the beginning of the softening branch in the torque-rotation diagram or to a change of its slope. Differently than for un-notched cylinders, after the peak the torque-rotation diagram decreases continuously and does not present any change in curvature. Like already mentioned for un-notched specimens, the diagrams present some scatter. The peak region can be rounded or, like observed in two tests of the first series, the torque decreases immediately after the peak. However, this occurs gradually and not with the drop observed in the tests conducted on un-notched cylinders. Furthermore, the softening branch can curve inwards or outwards. In the last case, like observed in two tests of the second series, the diagram shows an apex corresponding to the beginning of the softening. The tests conducted under a constant compressive force present a rather smooth torque-rotation diagram and the scatter band is narrow. In contrast with the un-notched cylinders, the peak load does not increase when the compressive force is constant during the complete test.

4 CRACK DETECTION BY IMPREGNATION

The experiments reported in the last sections show characteristic crack patterns, depending from the

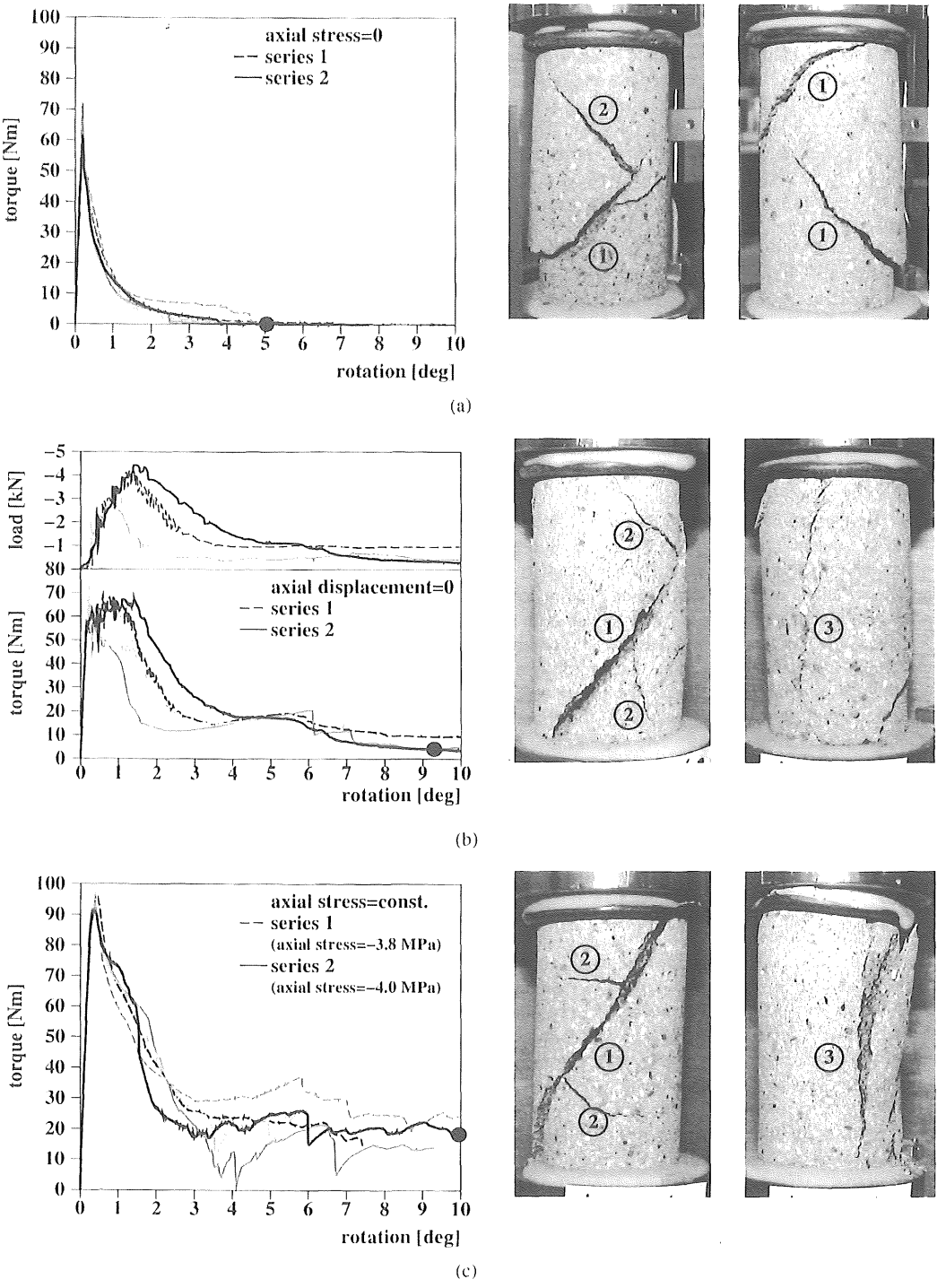

Figure 2. Experimental results of torsion tests conducted on un-notched cylinders under zero axial force (a), zero axial displacement (b) and constant compressive axial force (c).

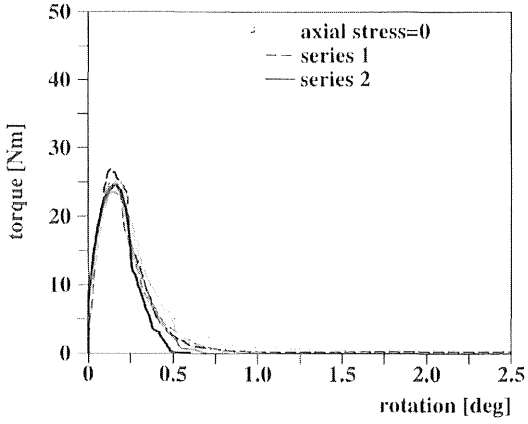

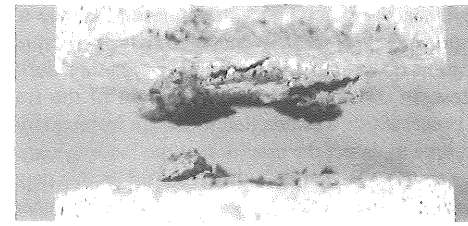

(a)

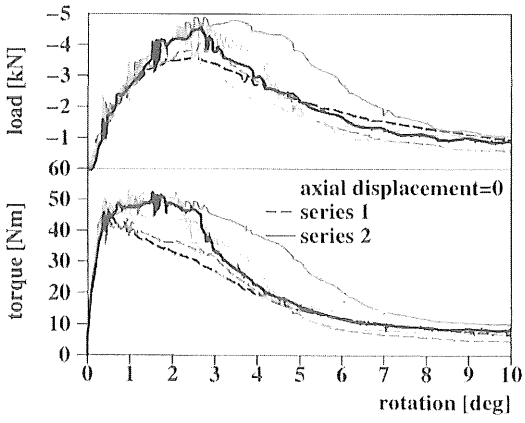

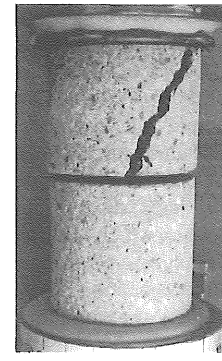

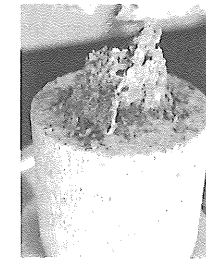

(b)

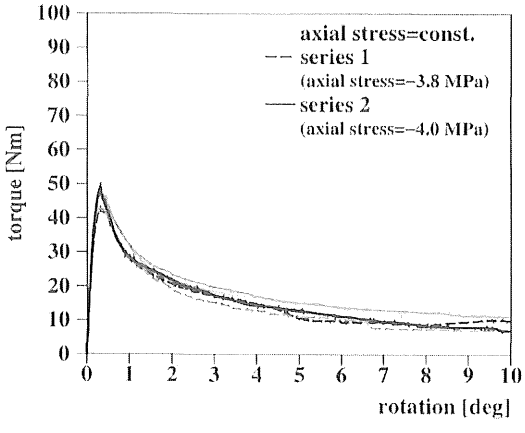

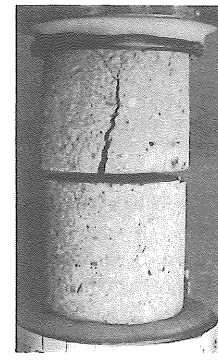

(c)

Figure 3. Experimental results of torsion tests conducted on notched cylinders under zero axial force (a), zero axial displacement (b) and constant compressive axial force (c).

adopted axial restraint. During the tests the cracks could be observed with the naked eye only at the cylinder's surface. Thus, no information concerning the fracture process inside the specimen could be obtained. On the other hand, after the end of the test the specimen was usually damaged, with consequent alteration of the cracks produced by loading during the test. In order to get a better insight of the fracture processes, it was decided to use an impregnation technique to detect the cracks at some loading stages. These tests are currently in progress and, in this paper, some preliminary results obtained on notched specimens subjected to zero axial displacement are shown.

4.1 Impregnation procedure

Once the desired loading stage is reached, the rotation is maintained constant setting the machine at hold position. In order to preserve the specimen in the same state as it is under loading, steel shells are bolted to the loading platens. Subsequently, the entire system comprising the specimen, loading platens and steel shells is debolted from the loading machine (Fig. 4a). Using a brass sheet, a container surrounding the specimen is built . The far ends of the brass sheet are shaped to form a hole for the entry of the fluorescenting epoxy used for impregnation (Fig. 4b). Next, the system is put inside an impregnation chamber, which is a transparent cylindrical container. First vacuum is made inside this cylinder. Then, the impregnation epoxy is injected in the specimen via a pipe, through the entry of the brass container. The specimen is completely impregnated when the epoxy is at the hole level and

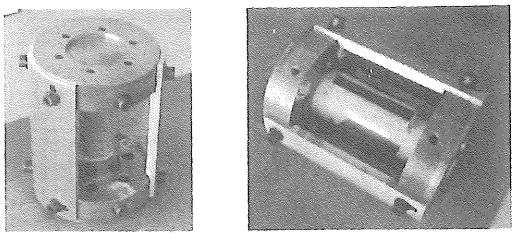

(a) (b)

Figure 4. Preparation of the specimen for impregnation.

no air bubbles appear anymore on its surface. The epoxy is left to harden for ≈12 hours. After, using a diamond saw, the specimen is cut from the loading platens and grinded at the ends. For a better handling of the specimen during subsequent slicing, it is glued to a steel block with height 40 mm. Then, each time, a slice with thickness ≈1.5 mm is sawn from the specimen. The new surface is grinded again. Afterwards, the specimen is positioned on a frame with a digital camera (3.3 MPixels resolution). The position of the specimen can be adjusted so that the pictures are all made at the same distance between camera end specimen surface. Images are taken under UV light. Next, the images are processed on a standard PC: first they are converted to 8 bit grayscale and subsequently inverted. As a result, the impregnated crack appears black.

4.2 Results

Two tests on notched cylinders (A and B) were conducted under zero axial displacement. The first test, on specimen A, was stopped after the peak torque was reached. The second test, on specimen B, was stopped after the maximum axial compressive force was reached. The experimental results are shown in Figure 5. For each test the crack patterns detected at different locations (defined by the coordinate Z) are shown. In both specimens, only one half of the specimen is cracked, while the other half is almost completely undamaged. In specimen A the bottom half was cracked, in B the top half. In the undamaged part only two tiny cracks are present which, at a certain location (Z=40 mm in specimen A, and Z=28 mm in specimen B), join each other. Already at the peak torque, cracks have developed through the specimen. Near the notch (Z=29 mm in specimen A, Z=37 mm in specimen B), these cracks isolate a core which appears to be crushed in specimen B. Most likely this zone corresponds to the apex of the conical failure surface typical of such tests. Between this zone and the end of the cylinder, cracks seem to develop from the cylindrical surface inwards, delimiting a region of intact material which becomes narrower in the direction of the notch. In specimen B, at Z=41 mm, such zone is pretty similar to the neighbouring zone already indicated as apex of the cone. Then, it appears clearly that a 'cone' like failure occurs also at the side of the cracked half cylinder opposite to the first cone. The two failure surfaces seem to touch each other. Such a crack pattern resembles very closely that in compression when friction between specimen and loading platens is present. In the case considered, at one end friction is produced from the bulk of material which confines the cylinder's core. At the other end confinement is produced by the loading platen to which the specimen is glued. Friction probably plays an important role in the fracture process. This is considered a key factor in future lattice analysis, where, so far, shear has not been included in the fracture law.

5 CONCLUSIONS

Torsion tests have been conducted on un-notched and notched concrete cylinders with diameter D=34 mm and height H=68 mm. Different axial restraints were used, namely: zero axial load, zero axial displacement and constant compressive load. The last two load-

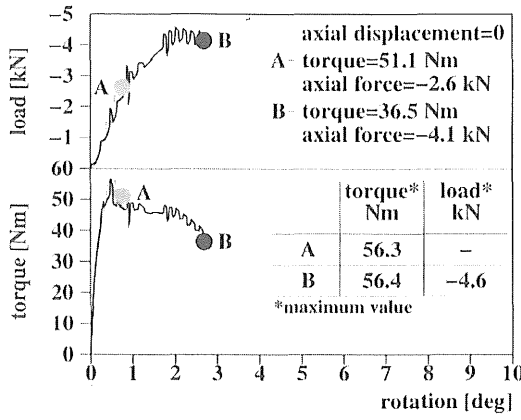

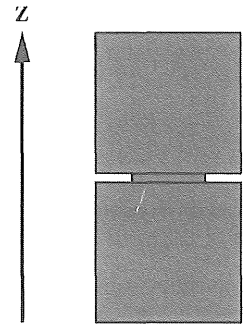

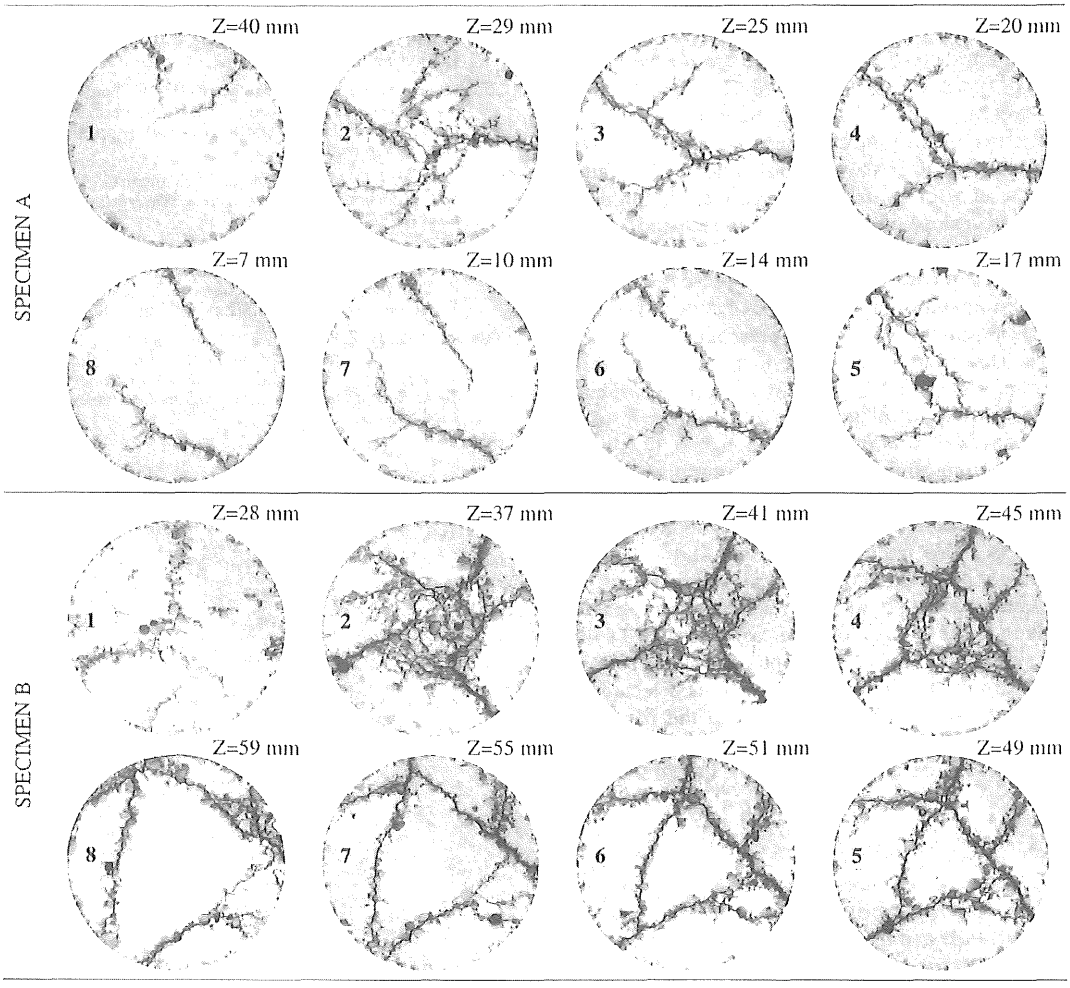

Figure 5. Crack detection by impregnation technique.

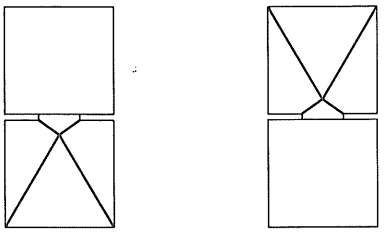

Figure 6. Schematical failure pattern in SPECIMEN A and SPECIMEN B.

ing conditions are somehow similar, since the constrained axial displacement produces as effect a variable axial compression. The crack pattern varies with the adopted axial restraint. The first to develop is a spiralling crack from which, in un-notched cylinders, "wing" cracks may depart. Vertical cracks appear if a compressive axial stress is applied. Localized failure within the notch height occurs in notched cylinders or a conical crack surface develops depending on the presence of an axial compressive stress. Like the crack pattern, the torque-rotation diagrams differ with axial constraint. In the tests on un-notched cylinders the presence of an axial compressive load produces changes in slope of the softening branch and, even, a new final increase of torque. The same kind of tests conducted on notched cylinders presented smooth torque-rotation diagrams. In case of constrained axial displacement the diagram can present a rounded peak zone. However, some scatter in the diagram shape was registered in this case. In all cases considered the sensitivity of torsion tests to the presence of an axial stress is confirmed, eventhough only a small amount of constraint is applied. Because of the chosen geometry and the complexity of the final crack pattern, it would be difficult to give an interpretation of the possible fracture mechanism during loading. Currently it is tried to detect propagation of cracks at different loading stages by means of an impregnation technique. As an example, the case of notched cylinder subjected to zero axial displacement has been included in the paper. The crack patterns detected immediately after the peak torque and the maximum compressive axial force show the formation of a "double cone" failure surface in only one half of the specimen.

AKNOWLEDGEMENTS

This research has been made possible through a grant from the Priority Programme Materials Research (PPM) and the Dutch Technology Foundation (STW), which is gratefully aknowledged. The authors are indebted to Mr. G. Timmers for his expert help in designing and performing the experiments.

REFERENCES

Bažant, Z. and P. A. Pfeiffer (1986). Shear fracture tests of concrete. *Materials and Structures (RILEM) 19*, 111–121.

Bažant, Z., P. C. Prat, and M. R. Tabbara (1990). Antiplane shear fracture tests (Mode III). *ACI Materials Journal 87*, 12–19.

Lilliu, G. and J. G. M. van Mier (1999). Analysis of crack growth in the brazilian test. In R. Eligehausen (Ed.), *Construction Materials: Theory and Application (H.W. Reinhardt 60^{th} birthday commemorative volume)*, pp. 123–137. ibidem.

Lilliu, G. and J. G. M. van Mier (2000). Simulation of 3D crack propagation with the lattice model. In *MaterialsWeek 2000*. http://www.materialsweek.org/proceedings.

Lingen, F. J. (2000). *Design of an object oriented Finite Element package for parallel computers*. Ph. D. thesis, Delft University of Technology.

Schlangen, E. (1993). *Experimental and numerical analysis of fracture processes in concrete*. Ph. D. thesis, Delft University of Technology.

Schlangen, E. and J. G. M. van Mier (1992a). Experimental and numerical analysis of micromechanisms of fracture of cement-based composites. *Cement and Concrete Composites 14*, 105–118.

Schlangen, E. and J. G. M. van Mier (1992b). Shear fracture in cementitious composites. Part II: Numerical simulations. In Z. P. Bažant (Ed.), *FraMCoS-I*, pp. 671–676. Elsevier Applied Science.

Vervuurt, A., J. G. M. van Mier, and Schlangen (1994). Analysis of anchor pull-out in concrete. *Materials and Structures (RILEM) 27*, 251–259.

Xu, D. and H. W. Reinhardt (1989). Softening of concrete under torsional loading. In S. P. Shah, S. E. Swartz, and B. Barr (Eds.), *Fracture of Concrete and Rock: Recent Developments*, pp. 39–50. Elsevier Applied Science.

Yacoub-Tokatly, Z., B. Barr, and P. Norris (1989). Mode III fracture - A tentative test geometry. In S. P. Shah, S. E. Swartz, and B. Barr (Eds.), *Fracture of Concrete and Rock: Recent Developments*, pp. 596–604. Elsevier Applied Science.